

# Dual time scales in simulated annealing of a two-dimensional Ising spin glass

Shanon J. Rubin, Na Xu,\* and Anders W. Sandvik†

*Department of Physics, Boston University, 590 Commonwealth Avenue, Boston, Massachusetts 02215, USA*

(Dated: September 1, 2018)

We apply a generalized Kibble-Zurek out-of-equilibrium scaling ansatz to simulated annealing when approaching the spin-glass transition at temperature  $T = 0$  of the two-dimensional Ising model with random  $J = \pm 1$  couplings. Analyzing the spin-glass order parameter and the excess energy as functions of the system size and the annealing velocity, we find scaling where the energy relaxes slower than the order parameter, i.e., there are two different dynamic exponents. We argue that such behavior arises as a consequence of the entropy-driven ordering mechanism within droplet theory. In the context of optimization, our study provides an example of robust dense-region solutions for which the excess energy (the conventional cost function) may not be the best measure of success.

A simulated annealing (SA) process [1] carried out on a system with a continuous phase transition exhibits scaling with the system size and the annealing velocity (the rate of change of the temperature  $T$  versus time). Following the seminal analysis by Kibble [2] and Zurek [3] (KZ) of the “freezing” of defects close to a critical point, a compelling picture has emerged of the combined effects of finite size and velocity on physical observables in SA [4–7]. The generalization of KZ scaling to quantum systems (where a system parameter is changed as a function of time at low  $T$ ) [8–10] has found applications in studies of cold atom systems [11, 12], and should be of relevance also in the quantum annealing (QA) [13] (or quantum-adiabatic [14]) approach to solving hard optimization problems by adiabatically evolving a programmable qubit system from a trivial to a complex ground state [15].

An untested application of classical KZ scaling is to systems with critical temperature  $T_c = 0$ . A prominent example of such a case is the two-dimensional (2D) Ising spin glass, which is interesting not only in its own right but also in the context of quantum annealing, e.g., the devices produced by D-Wave Systems [16] are laid out with a particular 2D connectivity. Numerous studies of 2D Ising spin glasses have been carried out recently in order to compare SA and QA, to gain insights into the nature of the quantum and thermal fluctuations in QA devices, and to develop methods for analyzing the efficiency of annealing protocols [17–20]. The KZ scaling formalism has not been applied, however. We here present such a study of the 2D Ising spin glass with bimodal couplings and find an unusual behavior where two different dynamic exponents govern the equilibration of the spin-glass (Edwards-Anderson, EA) order parameter and the excess energy, with the energy relaxing slower than the EA order parameter. We argue that this unusual behavior is a consequence of the entropy-driven EA ordering process within droplet theory [21, 22]).

The 2D Ising spin glass is defined by the Hamiltonian

$$H = \sum_{\langle ij \rangle} J_{ij} \sigma_i \sigma_j, \quad \sigma_i = \pm 1, \quad (1)$$

with random nearest-neighbor couplings  $J_{ij}$  drawn from,

e.g., a bimodal or normal distribution. The equilibrium properties of the bimodal  $J_{ij} = \pm 1$  model, which we focus on here, have been controversial. A long-standing issue has been to distinguish between exponential [23, 24] and power-law [25–27] scaling as  $T \rightarrow 0$ . The nature of the state at  $T = 0$  has also been difficult to ascertain. Until recently it was widely believed that the  $J_{ij} = \pm 1$  system does not harbor spin-glass order (unlike the model with normal-distributed couplings), only power-law decaying critical EA spin-spin correlations [28–30]. More recent studies [22, 31, 32] point to significant long-range order. In particular, Thomas *et al.* [22] evaluated the Pfaffian form of the partition function on larger lattices and lower temperatures than in previous Monte Carlo (MC) studies. A quantitative picture was presented for finite-size corrections to the long-range order at  $T = 0$ , power-law scaling at  $T > 0$ , and a size-dependent cross-over temperature  $T^*(L)$ , with  $T^* \rightarrow 0$  when  $L \rightarrow \infty$ , below which the discreteness of the couplings is important.

We here use out-of-equilibrium (SA) MC simulations to study the model with  $N = L^2$  spins on periodic square lattices. We generate the  $J_{ij} = \pm 1$  couplings independently with probability 1/2 and use bit representations for both the spins and the couplings (as discussed in detail in Supplemental Material, SM [33]), running 64 independent parallel simulations for each realization (sample) of the couplings and repeat for many samples. In addition to SA, where we go to system sizes up to  $L = 128$ , we have also used parallel tempering (PT) [34] to obtain equilibrium  $T \rightarrow 0$  results for smaller systems (up to  $L = 32$  for the energy and  $L = 24$  for the EA order parameter); see SM [33] for convergence tests. Although larger systems (with open boundaries) can be studied with ground-state methods [24, 35], proper thermodynamic averages of the EA order parameter, with equal weighting of degenerate states, are difficult to obtain [36].

We discuss the equilibrium PT results first because they will be important in the KZ scaling analysis. Averages were computed over millions of coupling samples for the smaller sizes and about  $10^5$  samples for the largest systems. The standard finite-size scaling ansatz [37] for a quantity  $A$  scaling as  $|T - T_c|^\kappa$  in the thermodynamic

limit is  $A(T, L) = L^{-\kappa/\nu} f[(T - T_c)L^{1/\nu}]$ , where the exponent  $\nu$  governs the correlation length,  $\xi \sim |T - T_c|^{-\nu}$ , and the scaling function  $f(x)$  must have the form  $x^\kappa$  for  $x \rightarrow \infty$  to ensure the correct thermodynamic limit. With this form, the singular behavior in a system of finite length is cut off at  $\xi \sim L$ , i.e., at  $|T - T_c| \sim L^{-1/\nu}$ . In the 2D  $J = \pm 1$  spin glass  $T_c = 0$  and a low size-dependent energy scale was identified,  $T^*(L) \sim L^{-\Theta_S}$ , where  $\Theta_S \approx 0.50$  is an exponent quantifying the entropy due to zero-energy clusters; flipping a cluster of linear size  $l$  changes the entropy by  $\Delta S \sim l^{\Theta_S}$  [22, 38]. The finite-size scaling relation then changes to

$$A(T, L) = L^{-\kappa\Theta_S} f(TL^{\Theta_S}). \quad (2)$$

Thomas *et al.* showed that the specific heat exponent is  $\alpha = 1 - 2/\Theta_S$  [22]. Then, at  $T = 0$ , Eq. (2) with  $\kappa = \alpha$  predicts that the finite-size energy correction (per spin) should be  $\Delta E_0 = E_0(L) - E_0(\infty) \sim L^{-2}$ . This form was obtained based on a different scenario in [24] and was consistent with data for periodic systems. In our PT simulations we generated a much larger number of samples for all systems up to  $L = 32$ , to obtain a more reliable estimate of the  $L^{-2}$  term. As shown in Fig. 1(a), the agreement with the prediction is excellent. The extrapolated infinite-size energy,  $E_0 = -1.40192(2)$ , is in good agreement with the best previous result,  $E_0 = -1.401938(2)$ , from open-boundary systems [35] (see also [24]). Using the more precise value to constrain the fit we obtain  $\Delta E_0 = aL^{-2}$  with  $a = 1.230(2)$ .

The EA order parameter is defined with two replicas (independent simulations with the same couplings) as

$$q = \frac{1}{N} \sum_{i=1} \sigma_i^{(1)} \sigma_i^{(2)}. \quad (3)$$

We evaluate  $\langle q^2 \rangle$  and extrapolate it to infinite size, as shown in Fig. 1(b). Since long-range order is expected at  $T = 0$ , the exponent  $\kappa = 0$  in Eq. (2) and the size dependence reflects a correction of the form [22]  $\langle q^2(L) \rangle - \langle q^2(\infty) \rangle \propto L^{-\Theta_S}$ . With data for  $6 \leq L \leq 24$  our independent estimate of the exponent is  $\Theta_S = 0.60(3)$  for even  $L$  and  $\Theta_S = 0.52(3)$  for odd  $L$ . Fixing  $\Theta_S = 1/2$ , as was also done in Ref. [22], fits for both even and odd sizes are good and mutually consistent for  $L \geq 9$ . The extrapolated order parameter is then  $\langle q^2(\infty) \rangle = 0.373(3)$ , which is roughly consistent with the previous estimate,  $\langle q^2(\infty) \rangle = 0.395(10)$ , from large systems at low but non-zero temperature [22].

Turning to the SA simulations, we measure the time  $t$  in the standard way in units of MC sweeps, where each sweep consists of  $N$  attempted Metropolis flips of randomly selected spins. Starting in equilibrium at  $T_{\text{ini}} = 8$ , we anneal to  $T = 0$  in  $t_{\text{max}}$  MC sweeps according to the following generic power-law protocol:

$$T(t) = T_{\text{ini}}(1 - t/t_{\text{max}})^r. \quad (4)$$

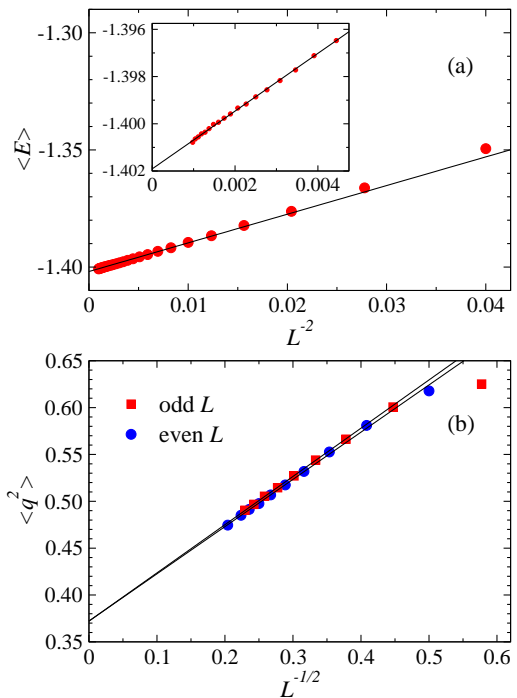


FIG. 1. (Color online) Equilibrium results for (a) the ground state energy graphed vs  $L^{-2}$  and (b) the EA order parameter vs  $L^{-1/2}$ . In (a) the results for  $L = 14 - 32$  were fitted to  $E_0 = -1.401938$  [35] plus a correction  $\propto L^{-2}$ . The inset shows data for the larger systems on a more detailed scale (where the error bars are similar to the symbol size). In (b), there are significant even-odd effects and  $L \geq 9$  data for even (blue circles) and odd (red squares)  $L$  have been individually fitted to constants plus  $L^{-1/2}$  corrections.

We define the velocity for  $r = 1$  as  $v = T_{\text{ini}}/t_{\text{max}}$  and use this definition of  $v$  as the inverse of the total annealing time also for  $r = 2$  and 4. We collect expectation values at the final temperature  $T = 0$ , using millions of samples for smaller sizes and several thousand for the largest systems. There is significant self-averaging and the error bars are small even for the largest sizes (much smaller than the plot symbols in the graphs below).

In standard KZ scaling, for a process stopping at the critical point, a singular quantity  $A$  depends on the velocity and the system size as  $A(v, L) = L^{-\kappa/\nu} g(v/v_{\text{KZ}})$ , where  $v_{\text{KZ}} \propto L^{-\bar{z}-1/(\nu r)}$  is the velocity separating fast and slow processes,  $\bar{z}$  is the dynamic exponent, and  $g \rightarrow \text{constant}$  when  $v \rightarrow 0$ . Variants of this ansatz have been confirmed in uniform systems [4–6] as well as in the 3D Ising spin glass (where  $T_c > 0$ ) [7]. It has proved to be a reliable way to extract the dynamic exponent, especially if  $T_c$  and  $\nu$  are known. If  $\nu$  is not known, it can be obtained along with  $\bar{z}$  by combining results for different  $r$  values in the protocol [6], and in principle  $T_c$  can be determined by using an extended scaling ansatz [4, 6].

The dynamic exponent relates the relaxation time scale  $\tau$  to the correlation length;  $\tau \sim \xi^{\bar{z}}$ . For given velocity, in the thermodynamic limit the correlation length saturates

at  $\xi_v \sim v^{-1/(\bar{z}+1/(\nu r))}$  and  $\xi_v \sim L$ , i.e.,  $v \sim L^{-\bar{z}-1/(\nu r)}$  demarks the “freezing” of the system. However, in the  $J = \pm 1$  model the entropy scale  $L^{-\Theta_S}$  present in the equilibrium should translate to velocity scaling as well. Expressed as a length scale, the entropic scale is,  $\xi_S \sim \xi^{1/(\nu\Theta_S)}$ , where presumably  $\nu \approx 3.4$  [39] as in the model with normal-distributed couplings (though this has been difficult to confirm [24, 27]). In any case,  $\nu\Theta_S > 1$  and  $\xi_S \ll \xi$ . In analogy with the equilibrium scaling [22], saturation in SA should then require  $L \sim \xi_v^{1/(\nu\Theta_S)}$  and we arrive at a modified KZ scaling form:

$$A(v, L) = L^{-\kappa\Theta_S} g(vL^{z+\Theta_S/r}), \quad z = \bar{z}\nu\Theta_S. \quad (5)$$

Here the renormalized dynamic exponent  $z$  directly gives the critical velocity  $v^*(L) \sim L^{-z-\Theta_S/r}$ , which is the original KZ ansatz with  $\nu$  replaced by  $1/\Theta_S$ .

Results for the EA order parameter in linear SA runs are shown in Fig. 2. For fixed velocity, the squared order parameter  $\langle q^2 \rangle$  drops rapidly with increasing system size. In Eq. (5) we have  $\kappa = 0$  as in the equilibrium, but since the correction to the asymptotic value of  $\langle q^2 \rangle$  is large we first divide it out based on the fitted form in Fig. 1(b). As shown in Fig. 2(b), we then rescale the  $x$ -axis by the size-dependent KZ velocity, optimizing the value of the exponent  $z + \Theta_S$  for the best data collapse for large systems and low velocities (see SM [33] for technical details and alternative scaling procedures).

The linear behavior on the log-log plot corresponds to velocities such that  $1 \ll \xi_S \ll L$ . In this regime  $\langle q^2 \rangle \propto L^{-d}$ , where  $d = 2$  is the dimensionality. Consistency with the  $L$  dependence in Eq. (5) then requires that  $g(x) \propto x^{-d/(z+\Theta_S/r)}$ . A line with the corresponding slope  $-2/(z + \Theta_S)$  (here  $r = 1$ ) in Fig. 2(b) shows perfect consistency with the data. Note that the data collapse procedure does not only involve this linear regime but also lower velocities where the behavior is turning toward a constant as equilibrium is approached. We do not go very far into this regime because of the exceedingly long running times for large systems. For smaller  $L$  we reach close to equilibrium and in SM [33] we show that the scaling there delivers a compatible exponent  $z + \Theta_S$ , with small size corrections. For  $r = 1$ , the exponent settles to  $z + \Theta_S = 8.83(4)$  as small systems are gradually excluded. At high velocity, the results in Fig. 2(b) deviate from the power law due to a cross-over [6], at an essentially size-independent velocity, reflecting the equilibrium behavior at the initial temperature.

Repeating these procedures for  $r = 2, 4$ , we can extract the exponents  $z$  and  $\Theta_S$ . As shown in Fig. 2(c), the  $r$  dependence agrees with the form of the KZ exponent, and we obtain  $z = 8.28(3)$  and  $\Theta_S = 0.55(6)$ . Fixing  $\Theta_S = 1/2$  does not significantly alter the value of  $z$ .

To study the singular part of the energy, we subtract the infinite-size value  $E_0$  from the velocity dependent energy  $E(v, L)$  and use  $\kappa\Theta_S = (|\alpha| + 1)\Theta_S = 2$  in Eq. (5).

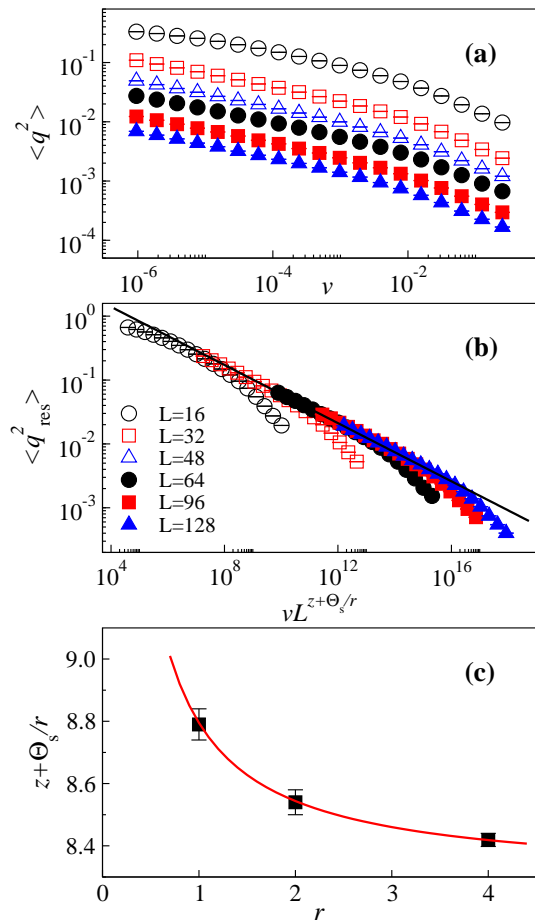


FIG. 2. (Color online) (a) EA order parameter squared vs the velocity in linear SA ( $r = 1$ ) runs for different system sizes (b) Velocity scaling, where  $\langle q^2 \rangle$  has been rescaled by the size correction,  $\langle q^2_{\text{res}} \rangle = \langle q^2 \rangle / (a + bL^{-1/2})$  with  $a$  and  $b$  the constants of the even- $L$  fit in Fig. 1(a), and the  $x$ -axis has been scaled with the optimal exponent  $z + \Theta_S = 8.83(4)$ . The line has the expected slope  $-2/(z + \Theta_S)$  in the power-law scaling regime. (c) The scaling exponent vs  $r$  along with a fit giving  $z = 8.28(3)$  and  $\Theta_S = 0.55(6)$ . The analysis included also several other system sizes within the range shown here.

We again optimize the data collapse with small systems and high velocities excluded. Fig. 3 shows  $r = 1$  results and similar  $r = 2, 4$  plots are presented in SM [33]. Combining the results for  $z' + \Theta_S/r$  for the different  $r$  values, we can again, as in Fig. 2(c), disentangle the exponents. Interestingly, here we obtain a clearly different dynamic exponent,  $z' = 10.32(7)$ , than  $z = 8.28(3)$  governing the EA order parameter, while  $\Theta_S = 0.5(1)$  is consistent with the previous value. Fixing  $\Theta_S = 1/2$  we can reduce the error bar on the dynamic exponent;  $z' = 10.31(4)$ . Using small systems close to equilibrium gives a similar value [33]. We also studied the lowest energy  $E_{\text{min}}$  reached in each SA run. Naturally,  $\langle E_{\text{min}} \rangle$  is somewhat lower than  $\langle E \rangle$  for each  $(L, v)$ , but the scaling exponent  $z' + \Theta_S/r$  is still the same. The scaling function  $g(vL^{z'+\Theta_S/r})$  is different for the two quantities [33].

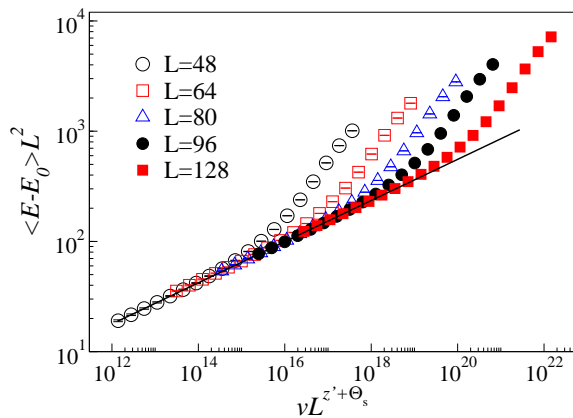


FIG. 3. (Color online) Mean energy above the infinite-size ground state energy  $E_0$  in  $r = 1$  SA runs. The results have been divided by the  $L^{-2}$  equilibrium size-dependence and the x-axis was rescaled according to the generalized KZ hypothesis (5), with  $\kappa\Theta_S = 2$  and the optimum-collapse value  $z' + \Theta_S = 10.80(8)$  of the scaling exponent. The line shows the expected slope  $2/(z' + \Theta_S)$  in the power-law regime.

The existence of two different dynamic exponents contradicts the standard picture of relaxation, where the slowest mode is associated with the fluctuation of the order parameter. The coupling of the energy to the order parameter (via defects) normally implies that the asymptotic energy relaxation is also determined by  $z$ . Thus, in the standard scenario, there is a single exponent governing the dynamic scaling of all quantities, except ones that are explicitly constructed to only sense *faster* modes.

The dual dynamic scales in the  $J = \pm 1$  model should be related to the phenomenon of droplet entropy stabilizing the EA order parameter when  $T \rightarrow 0$  in equilibrium. The backbone of the spin-glass cluster has a fractal dimension  $d_f < 2$  [40] and, thus, does not have long-range order on its own [22]. The ground states are strongly clustered within a small region (and its spin-reflected counterpart), which implies that these states are related to each other by flipping small (compared to the system size) droplets; flipping large droplet throws the system into atypical regions that are statistically insignificant in the thermodynamic limit. Although the absence of order at  $T > 0$  implies that low-energy excitations must be spread out over a large region of the configuration space, the ground state region should also have a much higher density of low-energy states than other regions (since these states can be obtained from the ground states by flipping small clusters). Thus, we have a region of typical ground states and low-energy states, illustrated in Fig. 4, and the large entropy drives the system toward this region under annealing. In the typical region, the EA order parameter, Eq. (3), has essentially the same distribution for replicas in low-energy states as for those strictly in ground states, and, therefore, the order parameter can converge even when a significant fraction of the replicas remain in excited states. Thus, our scaling re-

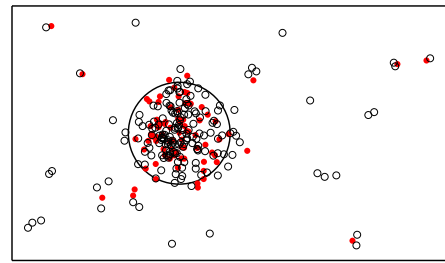


FIG. 4. (Color online) Conceptual illustration of the essential features of the energy landscape of the  $J = \pm 1$  model. Ground states (red solid circles) are clustered and typical states fall within a small region (large circle) of the configuration space. Low-energy excitations (black open circles) are predominantly located in the same region.

sults show that the final relaxation of the system involves transitions between excited states into ground states located in the same high-density region, and that the time scale for this is significantly longer (approximately by a factor  $L^2$ ) than that for reaching the high-density region.

Dynamic scaling is also interesting in the context of optimization. It has recently been argued that the best measure of optimization is not necessarily just the energy (the standard cost function), but the stability of the solution is also important and should be enhanced if the solution belongs to a dense region of similar solutions [41, 42]. A method was presented to enhance the ability to reach such regions, by using coupled replicas of the system. The 2D  $J = \pm 1$  Ising spin glass is an extreme case of a system harboring a dense region of low-energy states, and we have shown here that SA finds this region efficiently even without artificial replicating, as evidenced by the entropy-driven order parameter converging faster than the energy. In optimization, one may be willing to accept a slightly sub-optimal solution, as measured by the energy, for a solution in a dense region that can be found on a much shorter time scale. Clustering of solutions is also important when discussing the efficiency of QA protocols, where the measure of success is also ambiguous and solution stability may be a desirable feature. QA of systems with discrete coupling distributions may also be affected by dual time scales, due to mechanisms similar to those discussed here.

It would clearly be interesting to also study the KZ dynamics of the model with normal-distributed couplings, which has a unique ground state and likely different dynamic scaling. KZ scaling of  $T \rightarrow 0$  SA simulations can also be used in other systems that do not order at  $T > 0$ . Stimulated by the present work, the procedures were already applied to a planar vertex model encoding a class of reversible computing problems [43].

*Acknowledgments.*—We thank Anatoli Polkovnikov and Claudio Chamon for discussions. The research was supported by the NSF under Grant No. DMR-1410126. Computations were carried out on Boston University's Shared Computing Cluster.

- 
- \* naxu@buphy.bu.edu  
† sandvik@buphy.bu.edu
- [1] S. Kirkpatrick, C. D. Gelatt, Jr., and M. P. Vecchi, *Science* **220**, 671 (1983).
- [2] T. W. B. Kibble, *J. Phys. A* **9**, 1387 (1976).
- [3] W. H. Zurek, *Nature (London)* **317**, 505 (1985).
- [4] F. Zhong and Z. Xu, *Phys. Rev. B* **71**, 132402 (2005).
- [5] A. Chandran, A. Erez, S. S. Gubser, and S. L. Sondhi, *Phys. Rev. B* **86**, 064304 (2012).
- [6] C.-W. Liu, A. Polkovnikov, and A. W. Sandvik, *Phys. Rev. B* **89**, 054307 (2014).
- [7] C.-W. Liu, A. Polkovnikov, A. W. Sandvik, and A. P. Young, *Phys. Rev. B* **92**, 022128 (2015).
- [8] A. Polkovnikov, *Phys. Rev. B* **72**, 161201(R) (2005).
- [9] W. H. Zurek, U. Dorner, and P. Zoller, *Phys. Rev. Lett.* **95**, 105701 (2005).
- [10] J. Dziarmaga, *Phys. Rev. Lett.* **95**, 245701 (2005).
- [11] G. Lamporesi, S. Donadello, S. Serafini, F. Dalfovo, and G. Ferrari, *Nature Phys.* **9**, 656 (2013).
- [12] L. W. Clark, L. Feng, C. Chin, arXiv:1605:01023.
- [13] T. Kadowaki and H. Nishimori, *Phys. Rev. E* **58**, 5355 (1998).
- [14] E. Farhi, J. Goldstone, S. Gutmann, J. Lapan, A. Ludwig, and D. Preda, *Science* **292**, 472 (2001).
- [15] C.-W. Liu, A. Polkovnikov, and A. W. Sandvik, *Phys. Rev. Lett.* **114**, 147203 (2015).
- [16] M. W. Johnson *et al.*, *Nature (London)* **473**, 194 (2011).
- [17] S. Boixo, T. F. Rønnow, S. V. Isakov, Z. Wang, D. Wecker, D. A. Lidar, J. M. Martinis, and M. Troyer, *Nature Phys.* **10**, 218 (2014).
- [18] H. G. Katzgraber, F. Hamze, and R. S. Andrist, *Phys. Rev. X* **4**, 021008 (2014).
- [19] B. Heim, T. F. Rønnow, S. V. Isakov, and M. Troyer, *Science* **348**, 215 (2015).
- [20] H. G. Katzgraber, F. Hamze, Z. Zhu, A. J. Ochoa, and H. Muñoz-Bauza, *Phys. Rev. X* **5**, 031026 (2015).
- [21] D. S. Fisher and D. A. Huse, *Phys. Rev. B* **38**, 386 (1988).
- [22] C. K. Thomas, D. A. Huse, and A. A. Middleton, *Phys. Rev. Lett.* **107**, 047203 (2011).
- [23] J. Wang and R. H. Swendsen, *Phys. Rev. B* **38**, 4840 (1988).
- [24] I. A. Campbell, A. K. Hartmann, and H. G. Katzgraber, *Phys. Rev. B* **70**, 054429 (2004).
- [25] N. Kawashima, N. Hatano, and M. Suzuki, *J. Phys. A: Math. Gen.* **25** 4985 (1992).
- [26] H. Rieger, L. Santen, U. Blasum, M. Diehl, M. Jünger, and G. Rinaldi, *J. Phys. A: Math. Gen.* **29**, 3939 (1996).
- [27] H. G. Katzgraber, L. W. Lee, and I. A. Campbell, *Phys. Rev. B* **75**, 014412 (2007).
- [28] I. Morgenstern and K. Binder, *Phys. Rev. B* **22**, 288 (1980).
- [29] R. N. Bhatt and A. P. Young, *Phys. Rev. B* **37**, 5606 (1988).
- [30] J. Poulter and J. A. Blackman, *Phys. Rev. B* **72**, 104422 (2005).
- [31] T. Jörg, J. Lukic, E. Marinari, and O. C. Martin, *Phys. Rev. Lett.* **96**, 237205 (2006).
- [32] F. Roma, S. Risau-Gusman, A. J. Ramirez-Pastor, F. Nieto, and E. E. Vogel, *Phys. Rev. B* **82**, 214401 (2010).
- [33] See Supplemental Material following the main paper.
- [34] K. Hukushima, K. Nemoto, *J. Phys. Soc. Jpn.* **65**, 1604 (1996).
- [35] R. G. Palmer and J. Adler, *Int. J. Mod. Phys. C* **10**, 667 (1999).
- [36] A. W. Sandvik, *Europhys. Lett.* **45**, 745 (1999).
- [37] M. N. Barber, in *Phase Transitions and Critical Phenomena*, edited by C. Domb and J. Lebowitz, Vol. 8 (Academic, London, 1983).
- [38] L. Saul and M. Kardar, *Phys. Rev. E* **48**, R3221 (1993).
- [39] H. G. Katzgraber, L. W. Lee, and A. P. Young, *Phys. Rev. B* **70**, 014417 (2004).
- [40] A. K. Hartmann, *Phys. Rev. B* **77**, 144418 (2008).
- [41] C. Baldassi, A. Ingrosso, C. Lucibello, L. Saglietti, and R. Zecchina, *Phys. Rev. Lett.* **115**, 128101 (2015).
- [42] C. Baldassi, C. Borgs, J. Chayes, A. Ingrosso, C. Lucibello, L. Saglietti, and R. Zecchina, arXiv:1605:06444.
- [43] C. Chamon, E. R. Mucciolo, A. E. Ruckenstein, Z.-C. Yang, arXiv:1604.05354.

## SUPPLEMENTAL MATERIAL

### Dual time scales in simulated annealing of a two-dimensional Ising spin glass

Shanon, J. Rubin, Na Xu, and Anders W. Sandvik

#### Outline

We here provide technical details and some results complementing those in the main paper. Details of the simulated annealing and parallel tempering procedures are given in Sec. A and B, respectively. The scaling formalism underlying the extraction of the dynamic exponent is discussed in Sec. C. Illustrations for large systems in the power-law velocity scaling regime are presented in C-1, and in C-2 data for small systems approaching equilibrium are presented, to show the ability of the scaling form to account for both velocity regimes. In Sec. D we presented data-collapse plots for  $r = 2$  and  $r = 4$ , complementing the  $r = 1$  graphs shown in the main paper. The scaling of the minimum energy reached in the SA runs is discussed in Sec. E.

#### A. Simulated annealing

We code the spins  $\sigma_i = \pm 1$  of the model (1) as bits of long (64-bit) integers, thus using  $N$  integers  $I_i$  for a system of  $N$  spins and propagating 64 replicas of the same system (with the same random couplings). The bimodal couplings  $J_{ij} = \pm 1$  are also encoded as bits 0, 1, and most of the operations involved in computing energy differences for the Metropolis acceptance probabilities for single-spin flips (with the same spin considered in all replicas) can then be carried out simultaneously on all 64 replicas by using standard bit-wise logical operations on the stored integers.

In the beginning of each repetition of the SA, we generate new random couplings and initialize the spins to a random configuration. We then carry out 10 MC sweeps at the initial temperature  $T_{\text{ini}} = 8$ . We found that this small number of initial steps is sufficient for reaching very close to thermal equilibrium at this high temperature (and note that any deviation from equilibrium at this stage can be regarded as just a different initial state and will not affect the scaling when  $T \rightarrow 0$  at low velocities). In the subsequent SA run we carry out  $t_{\text{max}}$  MC sweeps and lower the temperature after each sweep according to the protocol in Eq. (4), carrying out measurements of the EA order parameter and the energy after the final  $T = 0$  sweep. To compute the EA order parameter (3) we form 32 pairs out of the 64 replicas and again use bit operations, thus obtaining 32 contributions from each measurement.

The safest way to ensure independent propagation of the replicas is to generate different random numbers for the final accept/reject step for each replica, in which case the generation of the random numbers consumes a large fraction of the computation time. Strictly speaking, uncorrelated replicas are required only when computing the EA order parameter; any other correlations are unbiased (provided that the random number generator is not flawed), thus not causing systematical error in the final results but potentially reducing the effective amount of statistical data. For example, if the same random number is used for each replica, if ever two replicas go into the same state they will stay in the same state for the remainder of the simulation, thus reducing the number of independent replicas. No statistical bias is introduced in computed mean values, however. Once the system size is reasonably large, it is very unlikely for replicas to lock to each other in this way, and one can safely use the same random numbers within the two groups of 32 replicas between which the EA order is computed.

#### B. Parallel tempering

In our PT simulations [34], we again use the bit representation but now all the bits  $b \in \{0, 63\}$  correspond to different temperatures on a uniform grid,  $T_b = T_0 + b\Delta_T$ . Attempts to swap spin configurations of runs at adjacent temperatures  $T_b, T_{b+1}$  are carried out after each MC sweep over the spins. The goal of the PT simulations is to obtain  $T \rightarrow 0$  equilibrium results for the EA order parameter and the ground state energy (results shown in Fig. 1). For the latter, we do not use the thermal energy average but simply keep track of the lowest energy reached in each run and average it over the coupling samples. We here present results showing proper convergence as the number of sweeps is increased.

We choose the lowest temperature  $T_0$  such that the  $T$  dependence of the EA order parameter is insignificant in the neighborhood of this temperature for the system sizes studied, i.e.,  $T$  is below the size-dependent entropic cross-over temperature  $T^*(L) \sim L^{-\Theta_s}$  [22] discussed in the main paper. The highest temperature should be high enough for the thermal fluctuations to migrate efficiently from high to low temperatures, thereby enhancing the ergodicity of the PT simulations relative to independent fixed- $T$  runs. Significant migration of the fluctuations also necessitates a sufficiently small  $\Delta_T$ , and in principle optimal simulations would also have  $\Delta_T$  decreasing with  $L$  and the number of temperatures increasing. Here we use 64 replicas and the spacing is  $\Delta_T = 0.04$  or  $0.02$ .

Figure S1 shows examples of the convergence of the EA order parameter and the lowest energy as functions of the number of sweeps in the PT simulations. We use the same number of sweeps for equilibration and for collecting data. The  $x$ -axis of Fig. S1 corresponds to the

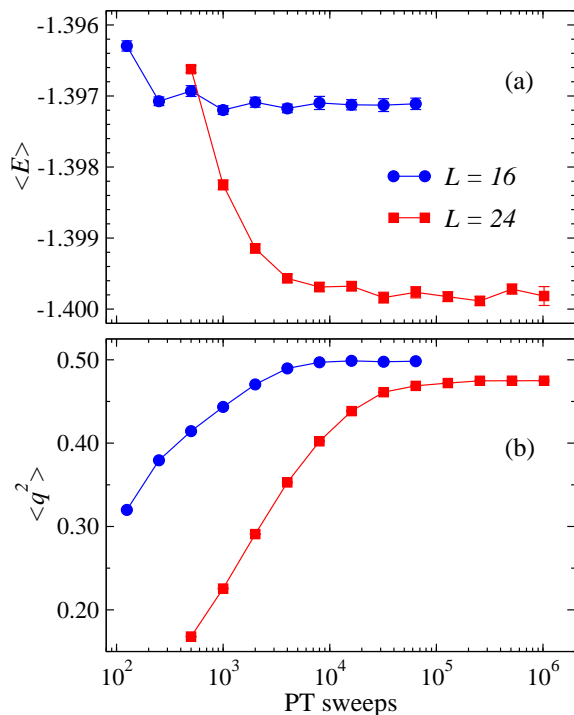


FIG. S1. (Color online) Convergence of PT results of the EA order parameter (a) and the excess energy (b) vs the number of sweeps for two system sizes. The lowest temperature was  $T_0 = 0.1$  and  $T_0 = 0.06$  for  $L = 16$  and  $24$ , respectively, and in both cases the temperature spacing was  $\Delta T = 0.02$ .

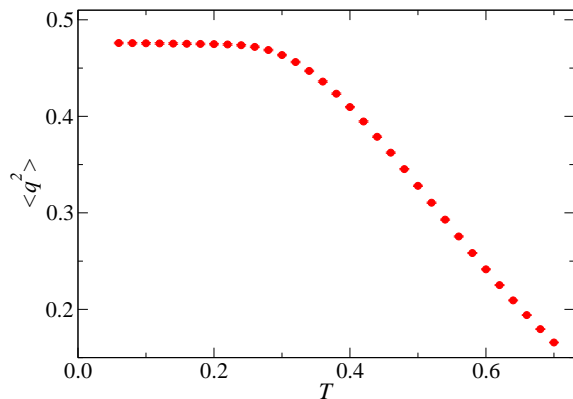


FIG. S2. Temperature dependence of the squared EA order parameter for  $L = 24$  in PT simulations with  $10^6$  sweeps for both equilibration and data collection.

sweeps for data collection only (i.e., the total number of sweeps is twice this number) and each successive point corresponds to doubling the number of sweeps. For these system sizes,  $L = 16$  and  $24$ , the ground state energy converges faster than the order parameter, but this trend is clearer for  $L = 16$  than  $L = 24$ . It is likely that the energy will converge *slower* than the energy for large sizes, as in the SA simulations (see also Sec. E below). We have not studied the scaling properties of the PT scheme.

For acceptable convergence, we require statistically indistinguishable results from at least the last two runs in

a series of runs such as those in Fig. S1. Based on this criterion we have converged results for  $\langle q^2 \rangle$  up to  $L = 24$  and for  $\langle E \rangle$  up to  $L = 32$ . To ensure that we obtain  $T \rightarrow 0$  results, it is also important to check the temperature dependence of the results. Fig. S2 shows results for  $L = 24$ , from PT runs with the largest number of sweeps [corresponding to the last point in Fig. S1(b)]. Here we can see that there is very little  $T$ -dependence below  $T \approx 0.25$ . We estimate that the very small remaining finite-temperature effect at  $T_0 = 0.06$  is much smaller than the statistical error.

### C. Data collapse procedures

According to the general non-equilibrium finite-size scaling form in [6], adapted to the present case where  $1/\nu$  is replaced by  $\Theta_S$ , the squared order parameter  $\langle q_{\text{res}}^2 \rangle$  can be written in the following way in three different regimes:

$$\langle q_{\text{res}}^2 \rangle \propto \begin{cases} \sum_n c_n (vL^{z+\Theta_S/r})^n, & v \lesssim v^*, \\ (vL^{z+\Theta_S/r})^{-x} = L^{-2}(1/v)^x, & v^* \lesssim v \lesssim 1, \\ L^{-2} \sum_n c_n (1/v)^n, & v \gtrsim 1, \end{cases} \quad (\text{S1})$$

where  $v^* = v^*(L) \propto L^{-(z+\Theta_S/r)}$  is the generalized KZ velocity separating the near-equilibrium and power-law scaling behaviors. Recall that  $\langle q_{\text{res}}^2 \rangle$  is the rescaled quantity obtained by dividing  $\langle q^2 \rangle$  by the multiplicative finite-size correction  $a + bL^{-\Theta_S}$ , with  $a$  and  $b$  corresponding to the fitted constants in Fig. 1 of the main paper, and this quantity approaches 1 for large system sizes (provided that the form of the correction is correct) in equilibrium ( $v \rightarrow 0$ ). The factors  $L^{-2} = L^{-d}$  in Eq. (S1) represent the overall size dependence in the limit where  $\xi_v \ll L$  and the exponent  $x$  has to be given by

$$x = \frac{2}{z + \Theta_S/r}, \quad (\text{S2})$$

in order for the two expressions on the middle line to be equal. The Taylor-expandable near-equilibrium behavior on the first line of Eq. (S1) should smoothly connect to the first power-law form on the second line, through a cross-over region in the scaling function  $f(vL^{z+\Theta_S/r})$  [Eq. (5) in the main paper]. In the high-velocity limit, the third case above, the behavior can be expressed as a series in  $1/v$ , and this series has to be smoothly connected to the form  $L^{-2}/v^x$  on the second line.

Forms analogous to Eq. (S1) hold for other singular quantities, where the rescaling on the left-hand side of Eq. (S1) always corresponds to dividing out the critical size-dependence in equilibrium, i.e., the factor  $L^{-\kappa/\nu}$  in Eq. (2) (and in principle finite-size corrections can also

be divided out, as we do here) and  $L^{-2}$  on the second and third lines should be replaced by  $L^{\kappa/\nu-2}$  (or, alternatively,  $L^{\kappa/\nu}$  should be left out on both sides). We here focus on the EA order parameter but the scaling procedures are completely analogous for other quantities, e.g., the excess energy for which we present some additional results in Sec. C-2.

For convenience we denote the often occurring generalized KZ exponent by  $\sigma(r)$ ,

$$\sigma(r) = z + \frac{\Theta_S}{r}. \quad (\text{S3})$$

One can use Eq. (S1) for given  $r$  to extract this exponent either from the high-velocity side, by fitting a straight line to  $\ln\langle q_{\text{res}}^2 \rangle$  versus  $\ln(1/v)$ , the slope of this line being the exponent  $x = 2/\sigma(r)$  in Eq. (S2), or by adjusting  $\sigma(r)$  so that  $\langle q_{\text{res}}^2 \rangle$  versus  $vL^{z+\Theta_S}$  in the power-law and equilibrium regimes collapse onto a common scaling function for different  $L$ . An analysis from the high-velocity side can include data only in the power-law regime, unless high-velocity corrections are taken into account. The data-collapse method potentially can lead to better statistical precision if a substantial amount of data are available in the low-velocity cross-over and equilibrium regimes, where the power-law scaling no longer holds.

To disentangle Eq. (S3) and obtain the exponents  $z$  and  $\Theta_S$  (if its value is not known or one would like to test consistency with a known value, as we do here), it is in principle sufficient to work with two different values of  $r$  in the annealing protocol, Eq.(4), and extract  $\sigma(r_1)$  and  $\sigma(r_2)$ . Here, as a further consistency check we use three different values,  $r = 1, 2, 4$ , and fit the resulting  $\sigma(r)$  to the expected form (S3) with  $z$  and  $\Theta_S$  optimized for the best fit. The procedure was illustrated in Fig. 2(c) in the main paper, and the error bars on the final results for the exponents were estimated by repeating the fitting procedure several hundred times with Gaussian noise added to the original  $\sigma(r)$  values. Here we give further details on the data-collapse procedures. Below, in Sec. C-1 we first consider  $\langle q_{\text{res}}^2 \rangle$  for large systems in the power-law regime, and in C-2 we discuss both the EA order parameter and the excess energy for smaller systems in the regime where equilibrium is approached.

### C-1. Data collapse in the power-law regime

We here take  $r = 1$  as an example and in the following simply use  $\sigma$  for  $\sigma(r = 1)$ . In Fig. 2(a,b) we already illustrated how data are collapsed by optimizing  $\sigma$ . To characterize the goodness of the data collapse, we fit a high-order polynomial to a set of data points  $\{\ln\langle q_{\text{res}}^2 \rangle, \ln(vL^\sigma)\}$  for different  $v$  and  $L$ , sweeping over  $\sigma$  on a dense grid and locating the optimal value (minimum  $\chi^2$  for the fit). If a satisfactory collapse,  $\chi^2/N_{\text{dof}} \approx 1$ ,

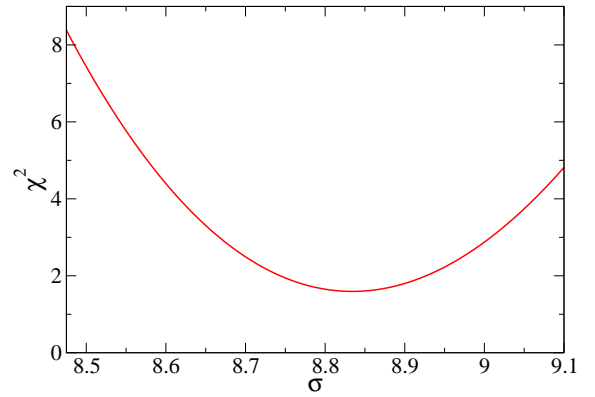


FIG. S3. Example for  $r = 1$  of the goodness of the linear fit of  $\ln\langle q_{\text{res}}^2 \rangle$  versus  $\ln(vL^\sigma)$  when the slope of the line fixed at  $-2/\sigma$ . The data used here is shown as the middle set (triangles) in Fig. S4. A scan is performed as a function of the exponent  $\sigma = z + \Theta_s$  and the minimum of  $\chi^2$  is identified for the optimum  $\sigma$ .

cannot be achieved we systematically eliminate small system sizes and/or high-velocity points until a statistically good fit is obtained. Typically tens of data points are left in the good fit. To estimate error bars, we perform bootstrapping, repeating the fitting procedure with many bootstrap samples and computing the standard deviation of the optimal  $\sigma$ .

Here, for illustration purposes we discuss a slightly simpler method for analyzing only the power-law regime and including only the three or four lowest available velocities for three system sizes;  $L = 72, 80, 96$ . For these sizes, even at the lowest velocity that we have studied,  $v = 8/t_{\text{max}} = 2^{-17}$ , the systems are far from equilibrium but, as we will show, they fall within the power-law scaling regime described by the middle line in Eq. (S1). Graphing on a log-log scale, we then expect all points to fall on a common line with slope  $x$  given by Eq. (S2) if the horizontal axis is appropriately rescaled as  $vL^\sigma$ . We use the required  $r = 1$  line slope  $-2/\sigma$  to constrain the fit to the form  $-(2/\sigma)\ln(vL^\sigma) + b$ , i.e., for given  $\sigma$  in the scaling procedure  $b$  is the only adjustable parameter. We scan over a dense grid of  $\sigma$  values, perform the constrained line fit for each case, and keep track of  $\chi^2$  to locate the minimum value; see Fig. S3 for an illustration. The optimum  $\sigma$  value is the result.

Alternatively, according to the second form of the middle line in Eq. (S1), we could also just consider  $L^2 \ln\langle q_{\text{res}}^2 \rangle$  versus  $\ln(1/v)$  and extract the slope  $x = 2/\sigma$  (and again a good  $\chi^2$  value would be an indication of being within the power-law scaling regime). The approach discussed here can, however, also be generalized to include low-velocity data, where the power-law scaling no longer holds but the behavior is described by the scaling function  $g(vL^\sigma)$ , of which the power-law constitutes the limiting form for large  $vL^\sigma$ . This latter part can be fitted to a line, and points deviating from it for smaller  $vL^\sigma$  can be simulta-

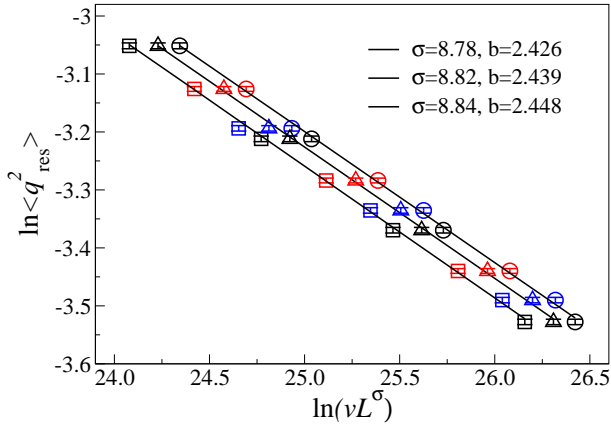


FIG. S4. Three different rescaled sets of data (indicated by different shapes of the graph symbols) obtained by bootstrap sampling of a large number of data bins for system sizes  $L = 72$  (black),  $80$  (red), and  $96$  (blue). The three lines are the best fits to the form  $\ln\langle q_{\text{res}}^2 \rangle = -(2/\sigma) \ln(vL^\sigma) + b$ , and the values of  $\sigma, b$  shown for each case corresponds to a  $\chi^2$ -minimum such as the one in Fig. S3.

neously fitted to a polynomial [6]. Here we just consider the linear part, while in Fig. 2 we also included lower- $v$  data but did not constrain the collapse by the line slope (instead obtaining the slope as a consistency check).

Figure S4 shows three different data sets along with the corresponding slope-constrained line fits. The middle set of points is the original data set, while the left and right sets correspond to the extreme cases out of 200 bootstrap samples. The standard deviation of  $\sigma$  computed from the bootstrap samples directly gives the error bar; in this case  $\sigma = \sigma(1) = 8.79(8)$ . This value is completely consistent with the value in the caption of Fig. 2, but the error bar is larger because only the linear regime was used and the number of data points is smaller.

Note that the same coupling realizations are used in SA runs with all velocities (where  $v$  is if the form  $2^{-n}$  for positive integers  $n$ ), and the data points for the same system size but different  $v$  are therefore strongly correlated (the sample-to-sample fluctuations being much larger than the MC sampling noise). The covariance predominantly corresponds to common up or down fluctuations of the value of the order parameter, and therefore the optimum line slope, as extracted above, is not significantly affected, and it is not necessary to use the full covariance matrix in the fitting procedure. The bootstrapping procedure properly account for the covariance since the same reandom bins are randomly chosen for all velocities for a given  $L$ .

Using the same system sizes and velocities and repeating the same procedures for  $r = 2$  and  $4$ , we obtain  $\sigma(2) = 8.52(6)$  and  $\sigma(4) = 8.48(7)$ . Combining these results and performing a fit to the expected  $r$  dependence of  $\sigma(r)$ , Eq. (S3), we obtain  $z = 8.35(7)$ , and  $\Theta_S = 0.42(8)$ , as shown in Fig. S5. These values are consistent with

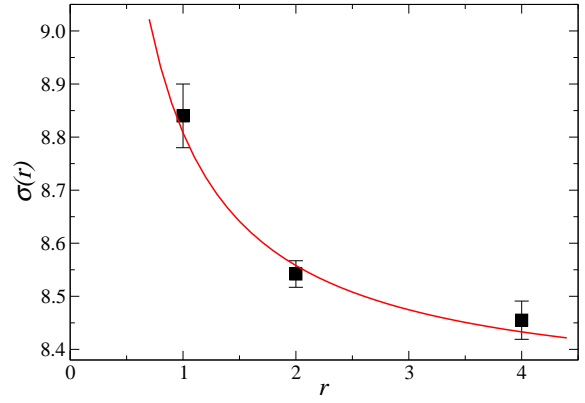


FIG. S5. The exponent  $\sigma(r)$  for  $r = 1, 2, 4$  along with a fit to the form (S3). The individual exponents (fitting parameters) are  $z = 8.35(7)$ , and  $\Theta_S = 0.42(8)$ , where the error bars were computed by repeated fits with Gaussian noise added [with standard deviation equal to the error bars on  $\sigma(r)$ ].

those presented in the main paper, but again the error bars are larger due to the smaller amount of data used. We can then conclude that the inclusion of also smaller sizes and lower velocities (including some data away from the power-law regime) in Fig. 1 did not change the exponents to a noticeable degree relative to the case here, where only large system sizes far from equilibrium were used. In the next section we go even deeper into the quasi-static regime.

### C-2. Scaling results for small system sizes

In the main paper and the previous section we discussed velocity scaling for systems sufficiently large for no significant subleading finite-size scaling corrections to remain (to within the statistical precision of the data). For large system sizes we can reach well into the power-law scaling regime (the linear part of the scaling function graphed on a log-log scale), but not very far into the cross-over into the regime where the systems approach and reach equilibrium, i.e., corresponding to the first line in Eq. (S1). It is important to test the scaling behavior also here, to make sure that the final relaxation stage is governed by the same dynamic exponent as the power-law regime.

Figure S6 shows  $r = 1$  results for lattice sizes in the range  $L = 8$  to  $32$ , with the exponent  $\sigma$  adjusted for best overall data collapse. Here the data-collapse procedure included all the system sizes shown, again excluding high velocities where no data collapse can be expected. We obtain the exponents  $\sigma = 9.01(5)$  and  $\sigma' = 10.9(2)$  for the EA order parameter and the energy, respectively. These values are very close to those obtained in Figs. 1 and 2 in the main paper,  $\sigma = 8.83(4)$  and  $\sigma' = 10.80(8)$ , respectively, demonstrating the stability of the results. We did not include the smallest systems in the analysis

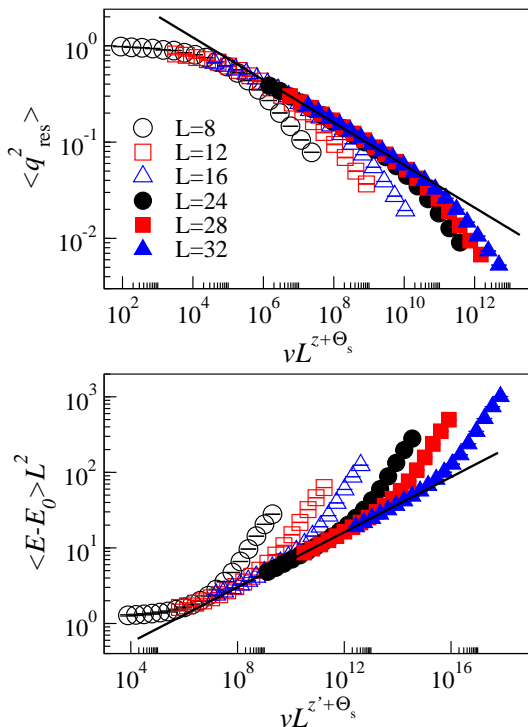


FIG. S6. Generalized KZ scaling analysis of the kind presented in Figs. 1 and 2 in the main paper, but for smaller systems for which the cross-over toward equilibrium can be observed. The velocity scaling exponents are  $\sigma = z + \Theta_s = 9.01$  and  $\sigma' = z' + \Theta_s = 10.8$  for the EA order parameter (upper panel) and the excess energy (lower panel), respectively. The lines have slopes  $2/\sigma$  and  $2/\sigma'$ , corresponding to the expected exponents in the power-law scaling regime.

in the main paper because, although the exponent values do not differ much, we can not obtain a statistically satisfactory value of the goodness of the fit ( $\chi^2$  per degree of freedom close to 1) when all data are included in a common fit, given the small error bars of the SA data and small but statistically significant effects of neglected finite-size scaling corrections for the smaller systems.

Given the good agreement we have demonstrated here and in the main paper between different system sizes and velocity regimes, we judge that the significant difference between the dynamic exponent for the excess energy and the EA order parameter,  $z' - z \approx 2$ , cannot be explained by neglected scaling corrections. The dual time scales are therefore a real aspect of the relaxation of the 2D  $J = \pm 1$  spin glass, and, as explained around Fig. 4 in the main paper, this unusual physics also fits naturally within the droplet theory of the 2D spin glass.

#### D. Results for $r = 2$ and $r = 4$

For completeness we here present the data for  $r = 2$  and  $r = 4$ , analyzed in the same way as the  $r = 1$  data in Figs. 2(b) and 3. Data-collapse plots for the EA order

parameter and the excess energy are presented in Figs. S7 and S8, respectively. The exponent values are given in the figure captions.

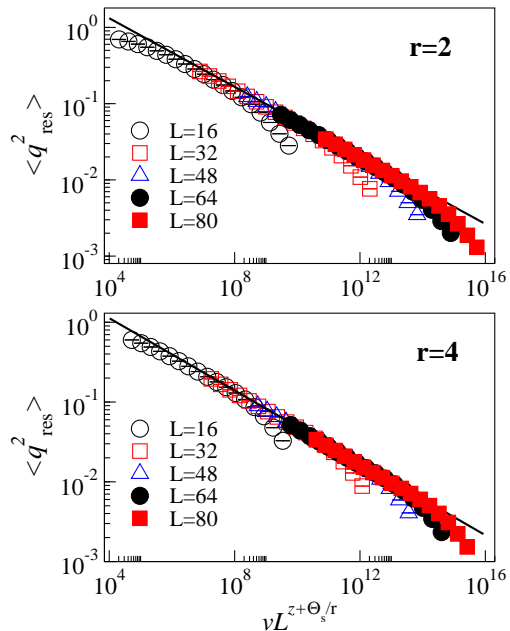


FIG. S7. Scaling collapse of the EA order parameter for  $r = 2$  and  $r = 4$ . The scaling exponents are  $\sigma(r = 2) = 8.57(3)$  and  $\sigma(r = 4) = 8.42(2)$ .

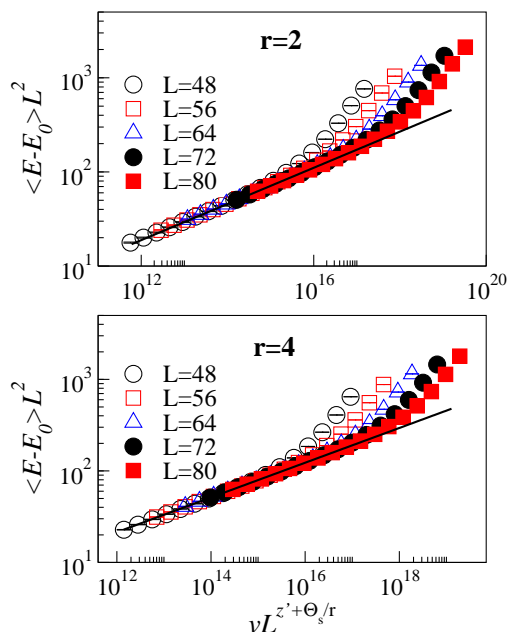


FIG. S8. Scaling collapse of the excess energy for  $r = 2$  and  $r = 4$ . The scaling exponents are  $\sigma'(r = 2) = 10.57(10)$  and  $\sigma'(r = 4) = 10.44(6)$ .

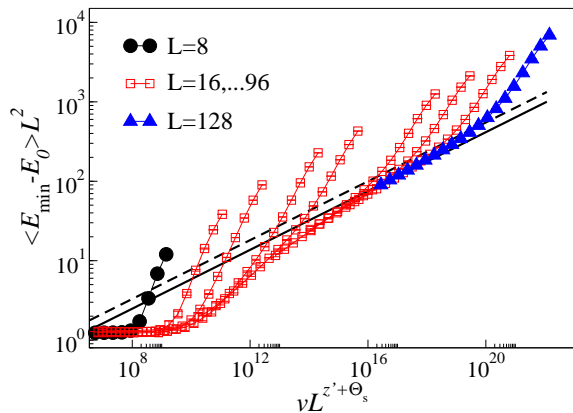


FIG. S9. Scaling of the minimum energy reached during any time in  $r = 1$  SA runs for  $L = 8, 16, 24, 32, 48, 64, 72, 96, 128$ . The exponents used for the rescaling of both the axis are the same as those in Fig. 3. The solid line has the expected slope  $2/(z' + \Theta_s)$  and is drawn in close proximity to the data for the largest system sizes—we expect that for even larger sizes the collapsed data will approach a line with this slope. The dashed line has the same parameters as the line in Fig. 3.

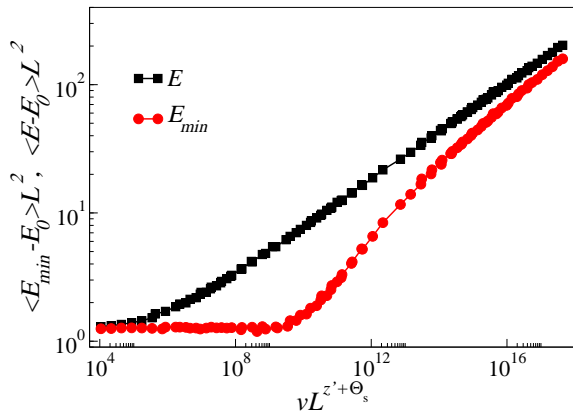


FIG. S10. Scaling function for the mean energy and the mean lowest energy in  $r = 1$  SA runs. Data points  $(v, L)$  for system sizes in the range  $L = 8$  to 128 were used, for each size excluding  $v$  points that deviate from the common data collapsed form. The value of the scaling exponent is the same as in Fig. 3;  $z' + \Theta_s = 10.8$ .

### E. Minimum energy

When optimizing with SA, it is better to keep track of the minimum energy  $E_{\min}$  reached during the entire run for each disorder sample (as we also do in the PT simulations discussed above in Sec. A). Even in very slow

annealings this energy is occasionally lower than the energy after the final MC step at  $T = 0$ . Therefore, the disorder-averaged  $\langle E_{\min} \rangle$  should be lower than  $\langle E \rangle$ . An important question then is whether the scaling of the two quantities is the same or not.

Figure S9 shows results for  $r = 1$ , scaled using the same exponents as in Fig. 3 in the main paper. The scaling collapse is still very good, and the optimized scaling exponent for this case is also statistically equal to the one obtained before. Overall the minimum energy values are, as expected, below those for the mean energy. With the range of system sizes used here we can see the full equilibrium behavior (the flat portion, where the value corresponds to the prefactor of the  $L^{-2}$  correction in Fig. 1 of the main paper) as well as the cross-over into the power-law scaling regime. In the graph we also draw a straight line with exactly the same parameters as the line drawn through the power-law scaling portion of the collapsed mean energy data in Fig. 3. In  $\langle E_{\min} - E_0 \rangle L^2$  we observe that larger systems are needed to observe the same slope—we see that the scaling function (onto which the data collapse) exhibits some curvature. Nevertheless, with increasing size the functional form appears to approach a line with the same slope as before. It is possible that it actually approaches exactly the same line (not just the same slope but also the same constant) as the one for  $\langle E - E_0 \rangle L^2$  in Fig. 3. If so the asymptotic power-law scaling of the two quantities would be exactly the same, and the advantages (in optimization applications) of monitoring  $E_{\min}$  instead of  $E$  would only appear as the behavior crosses over toward the equilibrium behavior.

We conclude that the minimum energy collected during SA runs converges to the ground state energy on the same time scale  $L^{z'+\Theta_s/r}$  as the convergence of the mean energy. The scaling functions are different, reflecting an overall lower value of the minimum energy than the mean energy for given scaled velocity  $vL^{z'+\Theta_s/r}$ . In Fig. S10 we show the two  $r = 1$  scaling functions explicitly, by combining data from other figures but only including the points that fall sufficiently close to a common scaling function. Here one can read off that  $E_{\min}$  ultimately converges (the curve flattens out to a constant) about  $10^4$  times faster than  $E$ . This factor depends on the details of how  $E_{\min}$  is computed in the simulations. In our case, we carried out 64 simulations in parallel for each coupling sample and monitored the lowest energy in any of these simulations. Clearly, upon increasing the number of parallel runs  $E_{\min}$  will converge faster, thus pushing the scaling function further to the right.